communications earth & environment

Article

A Nature Portfolio journal

https://doi.org/10.1038/s43247-025-02930-w

Particle properties and environmental factors control atmospheric transport and deposition of micro- and nanoplastics

Marianne Seijo[1], Michael J. Whelan[2], Todd Gouin[3] & Antonia Praetorius[1]

Atmospheric deposition plays an important role in the global distribution and long-range transport potential of micro- and nanoplastic particles. However, our mechanistic understanding of contributing processes remains limited. While similarities in wet and dry deposition processes can be expected between micro- and nanoplastics and well-studied natural and anthropogenic aerosols (e.g. mineral dust, pollen, black carbon), no holistic theoretical framework currently accounts for specific micro- and nanoplastic properties and their inherent heterogeneity. Here, we present an integrated mathematical model of atmospheric particle transport which incorporates micro- and nanoplastic properties (size, shape, density and surface characteristics, including effects of environmental ageing) based on theory and empirical data. We find that estimated micro- and nanoplastic half-lives in air can range from seconds to weeks, depending on particle characteristics, land surface type, surface wind speed, atmospheric stratification and precipitation. Micro- and nanoplastic particles with diameters of around 1 μm and fibres have the highest potential for long-range atmospheric transport.

Micro- and nanoplastic particles (MNPs), commonly defined as plastic particles ≤5 mm, represent a global environmental contaminant[1]. An important observation is that the major sources of MNPs, which often result from the fragmentation of larger plastic items, are strongly correlated with human activities[1]. The extent to which MNPs detected in remote regions originate from distal sources via long-range environmental transport, or from local emissions, however, remains a source of debate[2]. The development and application of mechanistic tools capable of describing MNP transformation and transport processes at the global scale is, thus, a priority in order to estimate MNP exposure in different environmental media and locations. Such tools would help to contextualise hazard data and assess ecosystem and human health risks.

MNPs are complex and highly heterogeneous entities[3–5]. They appear to be ubiquitously distributed in the environment, with the most commonly detected polymers having densities between 900 and 1600 kg m^{-3} [6], in various shapes, including spheres, fragments, films, and fibres. Depending on the polymer type, its use and functionality, MNPs can also often contain different (chemical) additives and fillers, which can potentially alter their density and/or surface properties (e.g. hydrophobicity). The physicochemical properties of MNPs can also change over time due to weathering and aging, which can influence their subsequent environmental fate, including additional fragmentation, aggregation and the formation of biological and mineral surface coatings. Elucidating the interplay between MNP properties (e.g. size, shape, density and ageing stage) and system conditions (e.g. environmental and meteorological conditions) is essential for estimating long-range environmental transport of MNPs.

There is increasing evidence that atmospheric transport processes may play an important role in the global distribution of MNPs[7–16]. The sources of MNPs released to the atmosphere are diverse[14], and include urban dust[17], tyre and road wear particles[8,18], erosion of landfill sites[19], agricultural soils[20], shedding from textiles[21–23], and release via sea spray[24–26]. Reported concentrations of atmospheric MNPs, size ranges and shapes vary greatly and are difficult to compare due to a lack of harmonised methods[27]. This limits our ability to parameterise and validate atmospheric transport models. Given the relatively rapid movement of air masses, which require days to weeks to traverse hemispheric distances, compared to ocean currents, which can take several years to travel comparable distances, transport of MNPs via the atmosphere may be more efficient than via the oceans[8,12,28].

A substantial body of research and literature has been generated over several decades, which has developed and applied mechanistic models to evaluate the atmospheric fate and transport of natural and anthropogenic particles (e.g. mineral dust, pollen, and black carbon)[29–32]. Such particles can influence global element cycling, long-range atmospheric transport (LRAT) of particle-bound contaminants and climate. Indeed, there

[1]Institute for Biodiversity and Ecosystem Dynamics (IBED), University of Amsterdam, Amsterdam, The Netherlands. [2]School of Geography, Geology and the Environment, University of Leicester, Leicester, UK. [3]TG Environmental Research, Sharnbrook, Bedfordshire, UK. e-mail: a.praetorius@uva.nl

have been various attempts to employ existing atmospheric particle transport models (e.g. FLEXPART, GEOS-Chem, CAM-CESM) to describe MNP transport, and to interpret monitoring data with an interest towards identifying potential emission sources[9,11,12,33–35]. A shortcoming with these models is that they typically only consider spherical particles of a relatively narrow size range and are unable to describe changes that may occur to MNP properties, such as aggregation or ageing effects. Although some MNP-specific environmental fate and transport models have been developed in recent years, these have primarily focused on describing the environmental fate and transport of MNPs in aquatic environments, rather than air[36–42].

Here, we explore the atmospheric transport of MNPs, with a particular focus on physical descriptions of deposition, which exerts the key control on atmospheric residence times[34,43] and, thus, LRAT. Specifically, we assess the combined impact of heterogenous plastic particle characteristics (size, shape, density, weathering state) and environmental factors such as land surface properties, surface wind speed, atmospheric stratification and precipitation, on dry and wet deposition. Although the actual concentrations and transport rates of MNPs are also influenced by emission (entrainment) rates, atmospheric residence times and the potential for LRAT of entrained material are mass-independent[44,45]. We, therefore, focus here on investigating the sensitivity of atmospheric residence times to deposition processes. The framework developed relies on the application of fundamental principles of physics but, where possible, parameterisation is further supported by data from empirical studies on the transport and atmospheric transformation of MNPs, as well as other particle types, including pollen, dust and aerosols.

The applied framework results in the observation that the estimated half-lives of MNPs in air can range from seconds to weeks, depending on their properties, land surface type, surface wind speed, atmospheric stratification and precipitation. MNPs with diameters of around 1 μm and fibres have the highest potential for long-range atmospheric transport.

Results and discussion

Deposition processes determine atmospheric residence times of MNPs

After emission to the troposphere from terrestrial or aquatic environments, MNPs can be transported through the air via diffusion and advection before being transferred back to the Earth's surface (Fig. 1). The main atmospheric removal processes for all airborne particles and associated chemical contaminants are dry and wet deposition[34]. Dry deposition involves particle settling onto or colliding with environmental surfaces due to gravitational forces. Wet deposition is essentially a wash-out process in which particles are scavenged by clouds, rain droplets or snowflakes and subsequently transported to the Earth's surface. The combined velocity of wet and dry deposition is the primary factor that influences the longevity of MNPs in the atmosphere and their potential LRAT.

Both dry and wet deposition velocities depend on a combination of particle properties (size, shape, density, surface characteristics) and environmental conditions, including surface wind speeds, the characteristics of the receiving surface (i.e. its affinity or stickiness for the particles) and atmospheric stratification. In addition, wet deposition is affected by the type and intensity of precipitation. Well-established theories have been developed for describing particle transport and deposition in the atmosphere, which have previously been applied to natural aerosols, such as mineral dust, pollen, ash[29–31,46] and particle-bound organic contaminants[47,48].

Here, we have adopted existing theories used in aerosol transport models to compile integrated mathematical descriptions of MNP dry and wet deposition, and expand them, where needed, to account for: (i) the wide range of MNP sizes (from a few nanometres to <5 mm); (ii) a diversity of particle shapes (especially the complexities stemming from fibres[13]) and (iii) the impact of polymer types and properties. These descriptions are then used to assess the relative importance of different particle- and environment-specific characteristics on MNP removal and identify the main contributors influencing atmospheric deposition of MNPs.

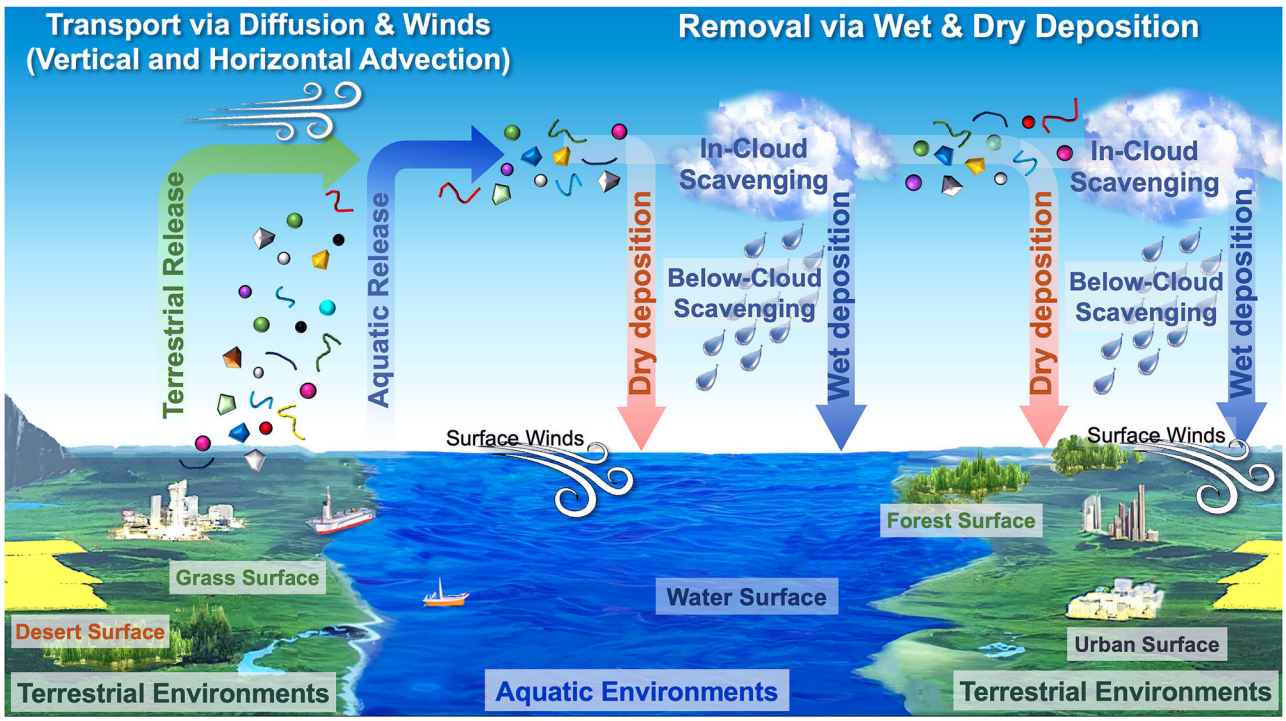

Fig. 1 | Release, transport and atmospheric removal processes of micro- and nanoplastic particles (MNPs). Two fundamental mechanisms govern MNP removal: dry deposition via gravitational settling and wet deposition during precipitation events or cloud activity. Different aquatic and terrestrial surfaces provide varying resistance to MNP deposition and surface winds can further affect deposition velocities.

Dry deposition of MNPs is largely driven by particle size and shape, land surface characteristics, surface winds and atmospheric stratification

Dry deposition of atmospheric particles is controlled by a combination of dry settling (i.e. gravitational settling) and surface resistance (or collection efficiency)[34,43,49]. Dry settling occurs as particles move downward in the air column under the influence of gravity, buoyancy and drag forces, as well as downward wind vectors. Surface resistance to deposition depends on the aerodynamic conditions near the deposition surface and on the interplay between depositing particles, the surface and surface winds. Here, different collection processes, i.e. Brownian diffusion, interception and impaction, play a role depending on particle size and surface characteristics (see also Supplementary Fig. 1).

The dry deposition velocity (v_d, in m s^{-1}) can be estimated from the terminal dry settling velocity (v_g), the aerodynamic resistance to deposition (R_a), and the surface resistance to deposition (R_s) as follows[49–51]:

$$v_d = v_g + \frac{1}{(R_a + R_s)} \quad (1)$$

In turn, v_g depends on particle size, shape, density and the resulting fluid dynamics (laminar or turbulent) due to a combination of gravitational, buoyancy and drag forces within the surrounding air. Different particle size ranges warrant the use of different deposition equations (Newton, Stokes or Brownian[51]) because different mechanisms influence the behaviour of the particle, depending on its size. The physics of dry deposition of MNPs is similar to that of other aerosols, such as mineral dust or pollen[52]: Settling of large particles is best described by the Newton equation, which considers mass and gravitational forces, as fluid inertia becomes relevant and gravity dominates settling (Supplementary Methods 1, Eq. S1). Intermediate-size particles experience viscous drag forces, which are best described by the Stokes equation (Supplementary Methods 1, Eq. S2). For very small particles—comparable in size to the mean free path of air molecules—Brownian diffusion is the predominant driver for settling (Supplementary Methods 1, Eq. S3).

MNPs can span a wide range of densities and the specific density of a given MNP type will determine their specific size threshold between Newton and Stokes settling modes. The most commonly detected MNPs range in density from around 900 kg m^{-3} (e.g. low-density polyethylene [LDPE]) to 1600 kg m^{-3} (e.g. polyvinyl chloride [PVC]), but densities up to 2200 kg m^{-3} are possible (e.g. polytetrafluoroethylene [PTFE]). We found the critical mean diameter above which the Newtonian regime applies to dry settling to be 72 ± 11 µm (at 20 °C, 1 atm), when accounting for the full density range of 900–2200 kg m^{-3}. For comparison, the mean cut-off between the Newtonian and Stokes regimes for pollen (with densities between 600 and 1200 kg m^{-3}) is around 85 ± 10 µm, and for mineral dust particles of higher density (ca. 2000–5000 kg m^{-3}) the size cut-off is around 52 ± 5 µm (Supplementary Fig. 2a). For particle sizes near to or below the mean free path of air molecules, the aerodynamic theory for the Stokes regime is no longer appropriate for describing particle motion. To address this, Cunningham[53] introduced a correction factor to Stokes' law, which should be applied to particles with diameters ≤ 17 µm to limit settling velocity errors for small particles to 1% (see Supplementary Methods 1, Eq. S4 and Supplementary Fig. 2b).

There is a clear effect of particle size on atmospheric half-lives of MNPs under dry deposition (i.e. in the absence of rain or snow) for individual, non-aggregated particles (Fig. 2). The longest half-lives of up to a few weeks are calculated for MNPs between 0.1 and 10 µm. Shorter half-lives are calculated for smaller MNPs (in the nanometre range; due to the dominance of Brownian motion) and the shortest half-lives (minutes to hours) for MNPs > 10 µm. Particle density also has some effect on dry settling, within the range of typical MNPs, i.e. from LDPE at 900 kg m^{-3} to PVC at 1600 kg m^{-3}, although the effect is smaller than for particle size (Supplementary Fig. 3a).

It has been demonstrated experimentally[54,55] that particle shape can strongly influence particle deposition. This is also evident in Fig. 2. Different shapes give rise to different drag forces and terminal dry settling velocities, which, in turn, influence the aerodynamics of settling[34,56,57]. To account for the impact of shape, empirically-derived Stokes shape factors

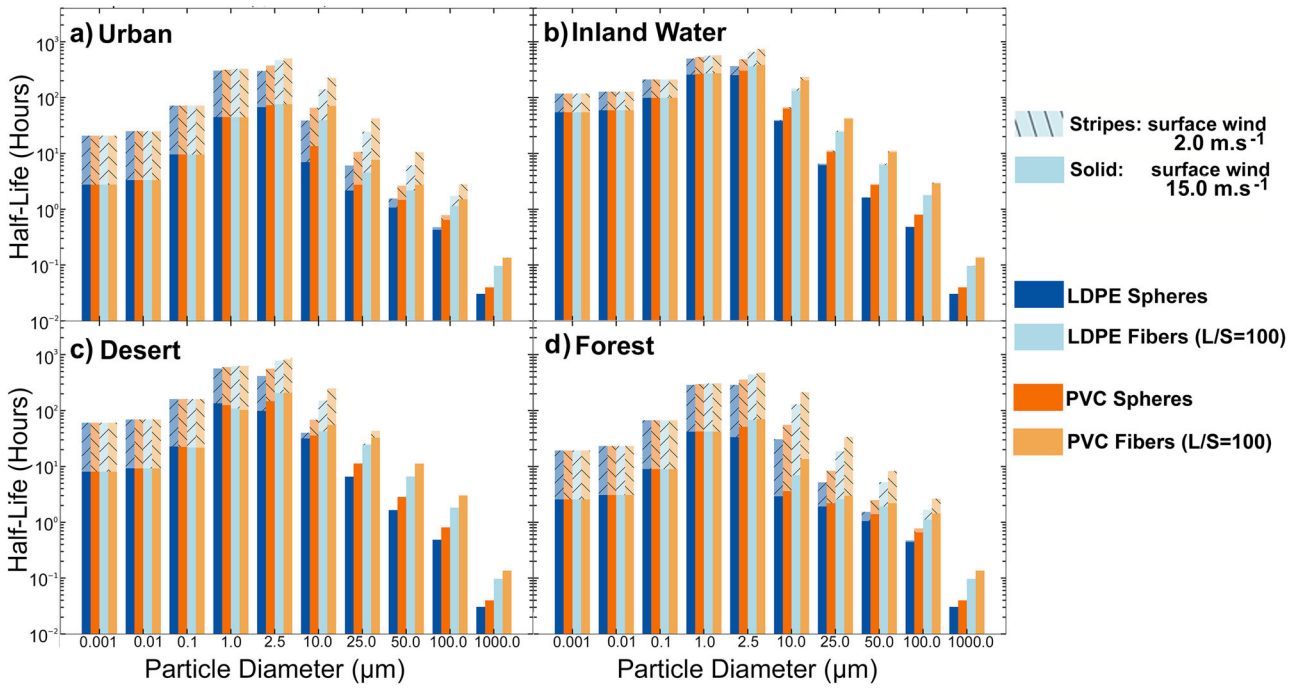

Fig. 2 | Atmospheric half-lives of micro- and nanoplastic particles (MNPs) under dry conditions. Half-lives of low-density polyethylene (LDPE, blue) and higher density polyvinyl chloride (PVC, orange) MNPs for a 1 km atmosphere under dry deposition conditions (i.e. in the absence of precipitation). Assuming deposition is a first-order process, half-life is defined as ln(2)*z/v_d, where z is the total height of the atmosphere and v_d is the dry deposition velocity, MNPs are either spheres (dark blue and dark orange) or fibres with an aspect ratio L/S (longest [L] over shortest [S] axis) of 100 (light blue and light orange). Four different land surfaces are shown (**a** urban, **b** inland water, **c** desert and **d** forest) and two surface wind velocities, u_s, of 2 and 15 m s^{-1}, respectively. Neutral atmospheric stratification is assumed.

Table 1 | Dimensions of volume-equivalent spheres and fibres used for comparison, with the same volume equivalence

Volume Equivalence (m^3)	Sphere Diameter (m)	Rod-Like Fibres		
		Aspect Ratio (*L*/*S*)	*L*, Longest dimension (length) (m)	*S*, Smallest dimension (diameter) (m)
5.24×10^{-28}	1×10^{-9}	100	1.88×10^{-8}	1.88×10^{-10}
5.24×10^{-22}	1×10^{-7}	100	1.88×10^{-6}	1.88×10^{-8}
5.24×10^{-19}	1×10^{-6}	100	1.88×10^{-5}	1.88×10^{-7}
5.24×10^{-16}	1×10^{-5}	100	1.88×10^{-4}	1.88×10^{-6}
6.55×10^{-14}	5×10^{-5}	100	9.41×10^{-4}	9.41×10^{-6}
5.24×10^{-13}	1×10^{-4}	100	1.88×10^{-3}	1.88×10^{-5}
5.24×10^{-28}	1×10^{-9}	50	1.19×10^{-8}	2.37×10^{-10}
5.24×10^{-22}	1×10^{-7}	50	1.19×10^{-6}	2.37×10^{-8}
5.24×10^{-19}	1×10^{-6}	50	1.19×10^{-5}	2.37×10^{-7}
5.24×10^{-16}	1×10^{-5}	50	1.19×10^{-4}	2.37×10^{-6}
6.55×10^{-14}	5×10^{-5}	50	5.93×10^{-4}	9.41×10^{-6}
5.24×10^{-13}	1×10^{-4}	50	1.19×10^{-3}	2.37×10^{-5}

Note that the cross-section of fibres equivalent to a sphere with a diameter of 1 nm falls within the angstrom range (~2 Å). This size is provided solely for comparison purposes and does not represent a realistic fibre size, unlike other ranges included in the table.

(Supplementary Table 3) are used to correct v_g for Stokes and Newton settling[58]. The corresponding equations were validated using observations of the settling velocities for different sizes and shapes of MNPs in column experiments (Supplementary Methods 1, Eq. S6 and S7 and Supplementary Fig. 4)[55]. Predicted settling velocities for spheres and cylinders agreed well with observations but our model slightly over-predicted velocities for fibres. This suggests that further work is needed to improve the model description of fibre behaviour in the atmosphere.

Fibres, in particular, have distinct aerodynamic characteristics and a multitude of possible orientations during settling, due to their specific geometry, linked to their aspect ratios (length/diameter) and their rigidity (Supplementary Table 4)[46,59–61]. Under otherwise identical conditions fibres have a reduced v_g compared to smooth spherical MNPs of the same equivalent volume (Table 1 and Supplementary Fig. 3b). This phenomenon is explained by buoyancy and surface area differences between fibres and spheres and is one of the most important factors explaining longer atmospheric residence times and transport distances of fibres (Fig. 2)[15,34]. Under otherwise identical conditions (and fixed volume equivalent), fibres with larger aspect ratios (length/diameter) will have a lower v_g (Supplementary Fig. 3b).

Other particle characteristics influencing dry settling include surface roughness (e.g. of weathered particles) and the fractal dimension and permeability of MNP aggregates, although these usually exert less control compared to size and shape. Nevertheless, their cumulative effects should not be overlooked. Pristine MNPs (i.e. particles not subjected to ageing and/or weathering) typically have smooth surfaces. However, exposure to temperature variations, photoaging, abrasion and adsorption of small molecules[62] can lead to an increase in surface roughness. Under dry settling conditions, weathered particles exhibit a lower gravitational settling velocity compared to pristine counterparts of equivalent diameter (Supplementary Fig. 3b). Increased surface roughness results in greater turbulence, which, in turn, heightens friction with the surrounding air and causes a reduction in settling velocity; a phenomenon also referred to as the 'golf ball effect' (as a golf ball's dimples prolong its time aloft and retard its descent compared to a smooth ball of comparable size and mass). The settling behaviour of aggregates also differs from that of individual particles and is influenced by aggregate structure, specifically the fractal dimension[63] (a geometric term, commonly used as measure of aggregate mass distribution in space), porosity (decreasing the density of the aggregate compared to an equivalent solid volume of the same material) and permeability of the aggregate to air[64]. Due to a reduction in air resistance, permeable fractal aggregates are predicted to settle faster than compact particles of the same size (see Supplementary Methods 1 and Supplementary Fig. 5 for more details).

In addition to particle-specific properties, environmental conditions—in particular land surface properties, atmospheric stratification and surface winds—strongly affect dry deposition velocities. The effect of land surface type[43,65] on particle deposition can be described using the concept of surface resistance (R_s), pertaining to particle collection efficiency. Some surfaces can be likened to selective filters, exhibiting differential affinities for the deposition of particles with a given size and surface characteristic. For gravitational settling alone we would expect an inverse relationship between particle size and atmospheric residence time (Fig. 3a). However, when resistance to deposition is accounted for, the relationship between particle size and residence time is more complex (Fig. 3b, c) with longest residence times predicted for particles around 1–2.5 µm in diameter. Importantly, ignoring surface resistance substantially underestimates the total deposition velocity of MNPs (note log scale for residence times).

Here we adopted the model by Zhang et al.[65] that considers 15 land use categories (LUCs) and 5 seasonal categories (Supplementary Table 6), to calculate the influence of land surface characteristics on dry deposition. This model has previously been incorporated into several large-scale aerosol and climate models[66–71]. It includes the effects of aerodynamic resistance R_a, surface resistance R_s and the rebound of particles from dry surfaces (see detailed equations in Supplementary Methods 2). Dry deposition is dominated by different processes for different particle sizes: gravitational settling, Brownian diffusion, interception, impaction and rebound (Supplementary Fig. 6). Rebound cannot be neglected for MNPs ≥ 1 µm (influenced by interception, impaction and gravitational regimes), whereas Brownian diffusion dominates for smaller particles. Gravitational settling becomes the main dry deposition mechanism for MNPs > 200 µm (based on Supplementary Fig. 6).

It is worth highlighting that an increase in the surface wind speed u_s promotes the settling of smaller MNPs (Figs. 2 and 3) by promoting the flux of MNPs coming into contact with and collecting on (rough) surfaces. The influence of surface wind speed differs for different land surface types (Supplementary Fig. 7): LUCs characterised by higher surface roughness, such as forests (LUC 2[65]) or urban areas (LUC 15[65]), have a lower surface resistance resulting in more efficient particle capture and a higher total settling velocity compared to smoother surfaces like deserts or inland waters (Fig. 2). For larger MNPs (>200 µm) this phenomenon competes with high gravitational settling and surface wind speed has a lower impact overall. Thus, MNP deposition at the global scale will differ based on the land surface types encountered in different regions.

Finally, atmospheric stability (linked to the air temperature gradient between land surface and higher altitudes [Supplementary Fig. 8]) can have a strong impact on dry deposition. Under unstable conditions (e.g. when near-surface air is much warmer than at higher altitudes) particle deposition increases due to increased vertical mixing of air masses (see pink area in Fig. 4). When atmospheric conditions are stable, the air can stratify with low vertical mixing, which decreases dry deposition.

Overall, dry deposition of MNPs is slowest for particles with diameters around 1 µm (Figs. 2 and 4). For these sizes, particles are not small enough for an efficient Brownian diffusion or big enough to be efficiently intercepted, impacted, or settled gravitationally. This implies that particles around 1 µm have the longest atmospheric half-lives (up to a few weeks under dry conditions). This finding is aligned with known trends for atmospheric aerosols[56].

Precipitation events accelerate removal, especially for very small and very large MNPs

Wet deposition refers to the removal of particles from the atmosphere through scavenging by aqueous phases (rain, fog, snow and hail). This can occur both within clouds and below clouds. In below-cloud scavenging

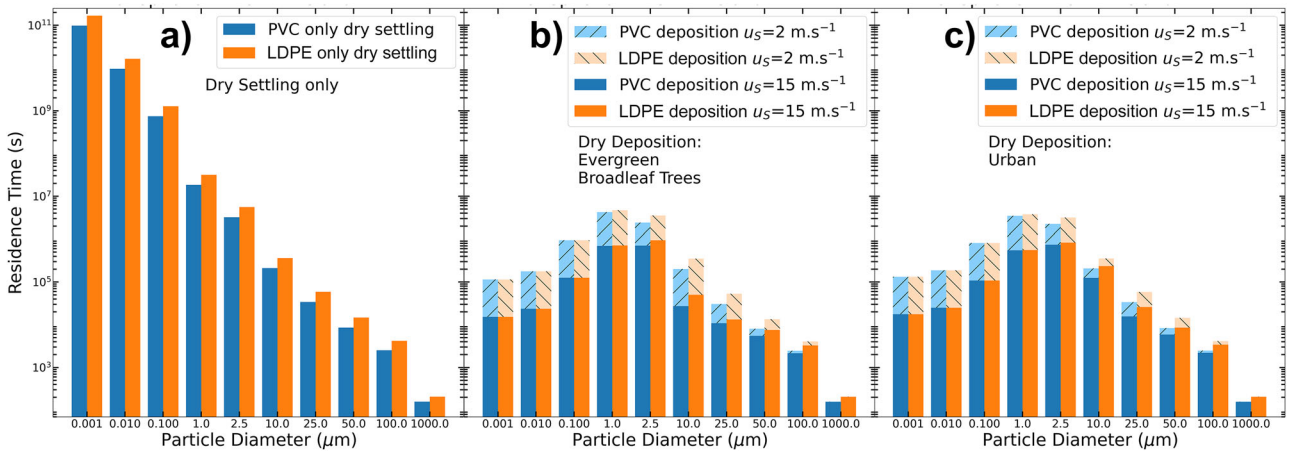

Fig. 3 | Impact of surface resistance on micro- and nanoplastic particle (MNP) deposition. Variation of MNP atmospheric residence time as a function of particle diameter for low-density polyethylene (LDPE) and polyvinyl chloride (PVC), based on **a** pure dry settling and dry deposition to **b** evergreen broadleaf trees or **c** urban surfaces, with surface winds u_s of 2 m s^{-1} (corresponding to a light breeze in the Beaufort Wind Scale: force 2) and 15 m s^{-1}.

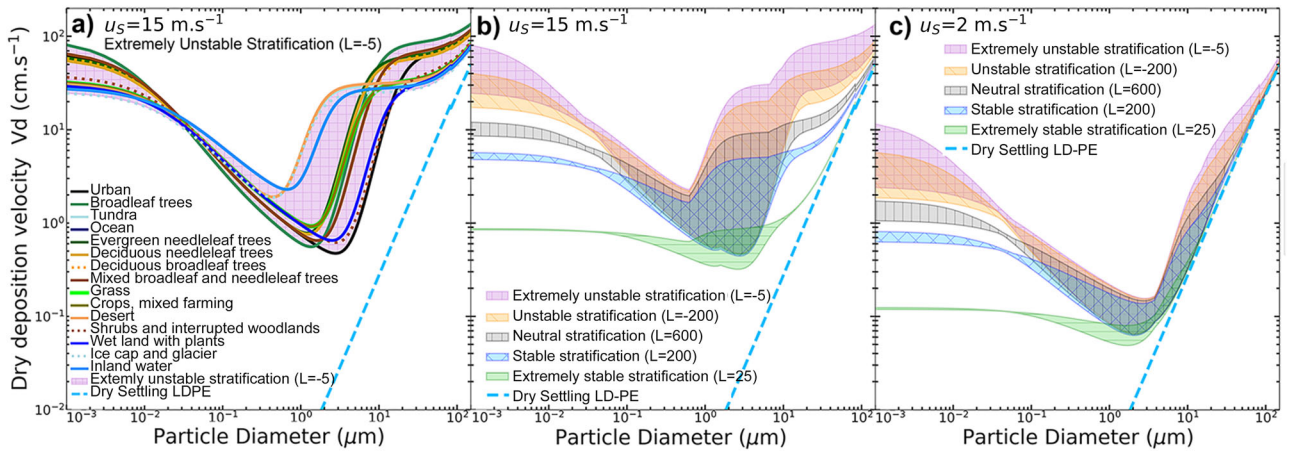

Fig. 4 | Micro- and nanoplastic particle (MNP) dry deposition under different atmospheric stratification conditions and surface winds. a Variation in dry deposition velocity as a function of low-density polyethylene (LDPE) diameter and Land Use Category (LUC) with a surface wind of u_s = 15 m s^{-1}, season: midsummer with lush vegetation, extremely unstable stratification. The area in pink between curves is used to highlight the impact of stratification; **b** variation in dry deposition velocity as a function of LDPE diameter and stratification (area representation between curves as in (**a**), surface wind u_s = 15 m s^{-1}, season: midsummer with lush vegetation; **c** variation in dry deposition velocity as a function of LDPE diameter and stratification (area representation between curves as in (**a**), u_s = 2 m s^{-1}, season: midsummer with lush vegetation.

particles are removed via collision with falling precipitation (rain, snow or hail). Here, we focus specifically on rain as the dominant form of global precipitation. The general principles of MNP removal by snow and hail are similar but are described using different equations due to differences in geometry and states of the precipitation[34]. In-cloud scavenging is the capture of particles by cloud droplets through collision or when particles act as cloud condensation nuclei (CCN), initiating condensation and droplet coalescence, or ice-nucleating particles (INPs), followed by settling with rain or snow (Fig. 5)[62].

The processes driving wet deposition strongly depend on meteorological conditions, particularly the intensity of precipitation, the size distribution of the precipitate, and the cloud characteristics, as well as on particle properties. During precipitation, when wet and dry deposition are additive, wet deposition leads to a more efficient removal of MNPs from the atmosphere, with calculated half-lives of the order of seconds to minutes for MNPs >10 μm and hours for MNPs around 1 μm (Fig. 6). Half-lives for MNPs <1 μm are also of the order of hours during precipitation events and typically at least one order of magnitude lower than under dry conditions.

Precipitation intensity has a strong impact on wet deposition velocities. Atmospheric half-lives of MNPs decrease exponentially with increasing intensity from light (here 0.5 mm h^{-1}) to heavy (here 10.0 mm h^{-1}) (Fig. 7). The time-dependent removal of MNPs by below-cloud scavenging can be described as a first-order decay process[72]:

$$\left.\frac{dC}{dt}\right|_{BCS} = -\lambda_p C \quad (2)$$

where C is the atmospheric concentration of MNPs (μg m^{-3}) and λ_p is the scavenging coefficient (s^{-1}), which depends on the size distribution and terminal velocity of the precipitate. The size of precipitate can vary between a few μm to up to 5 mm[51,52]. The collection efficiency of MNPs via below-cloud scavening depends on the interaction between MNP properties and precipitate sizes, because different physical collection mechanisms dominate for different size fractions. These include Brownian diffusion, interception, and inertial impaction. In addition, electroscavenging, thermo- or diffusiophoresis may also be important, depending on the size and

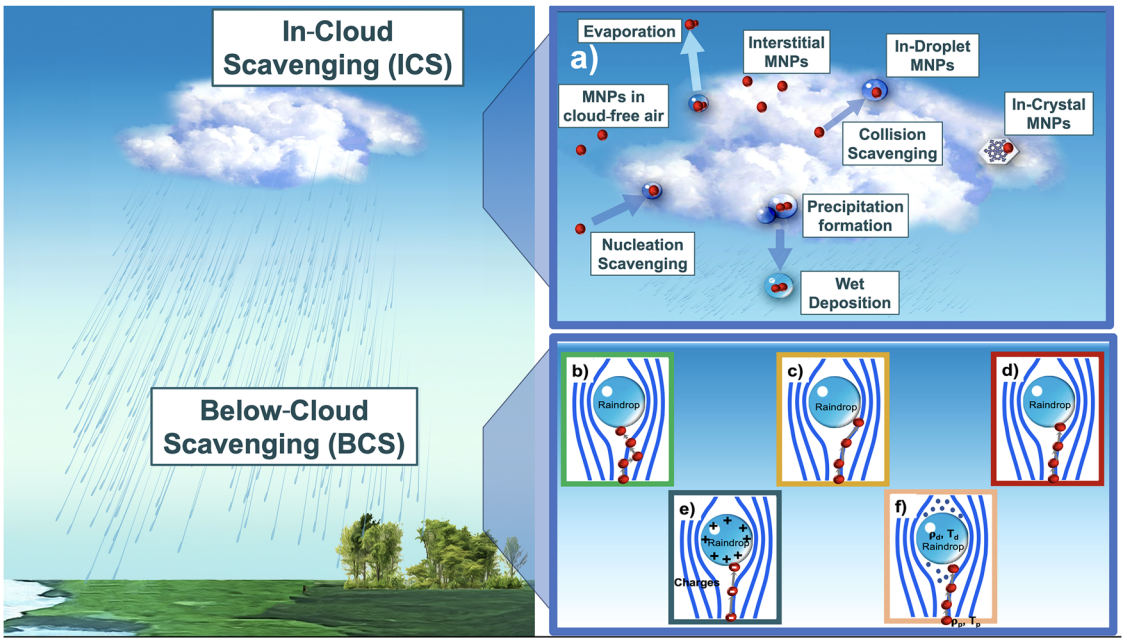

Fig. 5 | Wet deposition processes. Illustration of wet deposition via in-cloud scavenging and below-cloud scavenging. **a** In-cloud scavenging is controlled by several different mechanisms depending on the nature of the cloud and the particles under consideration[92,93]. Below-cloud scavenging will depend on particle and droplet sizes shown here for **b** small particles undergoing Brownian diffusion, **c** particles around 1 µm subject to interception, and **d** large particles subject to inertial impaction. **e** illustrates electroscavenging and **f** illustrates thermophoresis and diffusiophoresis.

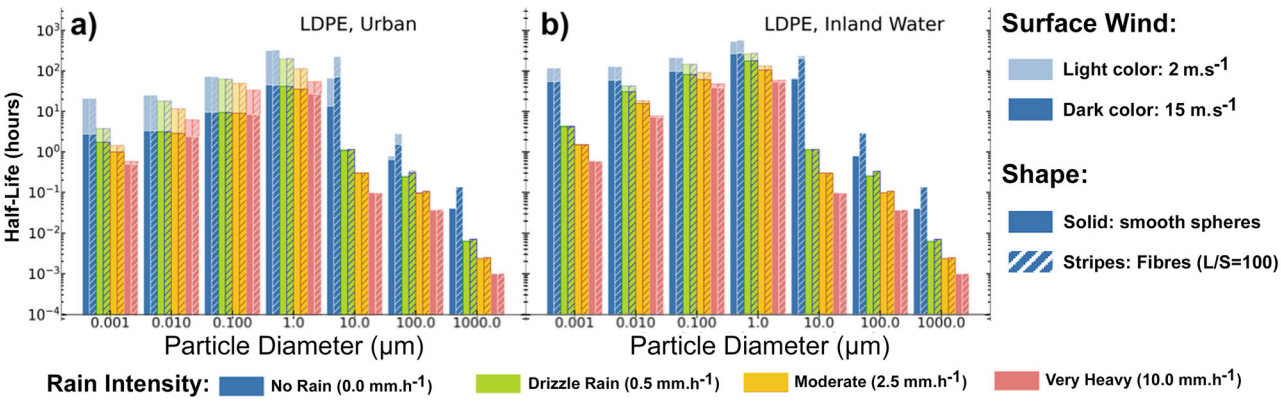

Fig. 6 | Atmospheric half-lives of micro- and nanoplastic particles (MNPs) under precipitation conditions. Half-lives of low-density polyethylene (LDPE) spheres and fibres settling from a 1 km atmospheric height during a precipitation event (i.e. combined dry and wet deposition), with two different surface wind velocities (u_s = 2 m s^{-1} and u_s = 15 m s^{-1}) and three different rain intensities (drizzle, moderate and heavy rain). Two different land surfaces are shown (**a** urban and **b** inland water). Two additional land surfaces (desert and forest are included in Supplementary Fig. 9.

composition of the MNPs (see Fig. 5 and Supplementary Methods 3). For precipitate of around 2 mm in diameter (typical for very heavy rain events) the collection efficiency of MNPs exhibits a distinct minimum for a diameter of 1 µm (Supplementary Fig. 12). This is reflected in longer wet deposition half-lives (Figs. 6 and 7). For MNPs of different polymer types, differences in wet deposition velocity (Fig. 7) are mostly driven by differences in thermal conductivity (Supplementary Table 7), which impacts scavenging by thermophoresis, rather than by differences in polymer density.

In-cloud scavenging can, in theory, also remove MNPs from the atmosphere[34]. It is governed by two distinct mechanisms: collision scavenging of MNPs by waterdrops and nucleation scavenging, which involves MNPs acting as CCN or INPs in the water-saturated atmosphere (Fig. 5)[62]. An important factor governing cloud condensation is relative humidity (RH). In supersaturated air (RH > 100%), droplets can grow rapidly around CCN[51,73], and then be removed by wet deposition. The likelihood of particle nucleation in a supersaturated environment depends on particle size, the hydrophilicity of its surface, and the supersaturation value RH. This is captured by the critical supersaturation S_c of a particle, which refers to the minimum level of supersaturation required for a particle to initiate nucleation, determined by the Köhler equation[74,75].

Pristine MNPs are typically very hydrophobic. As a result, water cannot condense on their surface in the range of supersaturation S generally observed in natural clouds (S between 1.0 and 1.01, with a probable absolute maximum value of S in natural clouds of 1.03 [RH = 103%]). To act as CCN, a low contact angle $\theta \leq 12°$ between the particle surface and water is required. Very hydrophobic surfaces exhibit contact angles > 90° and thus have low wettability. Photoaging increases wettability (decreased contact angles, as measured for several polymers by Huang and Wang[76], see also

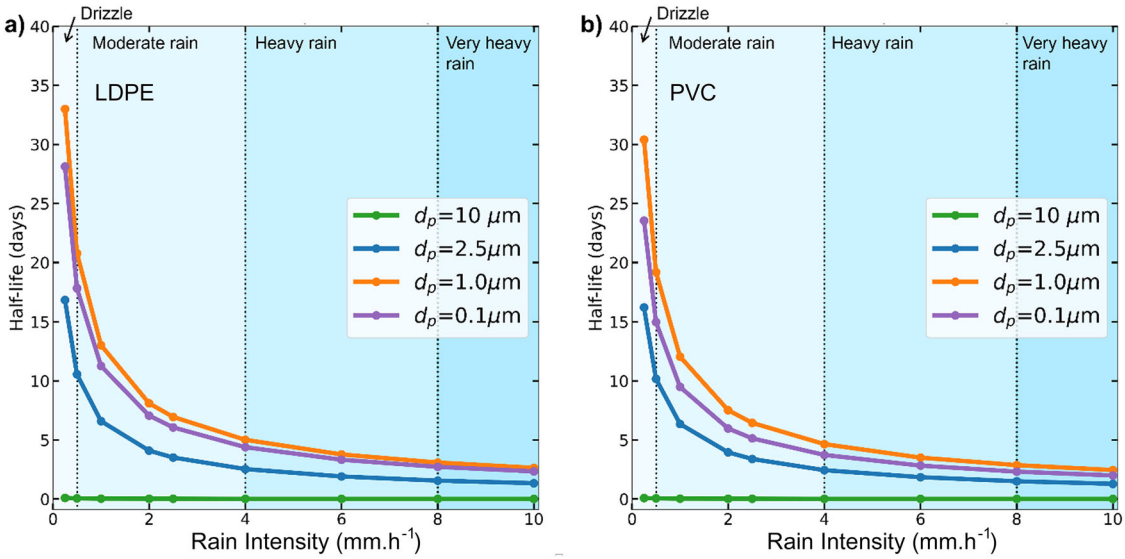

Fig. 7 | Impact of precipitation intensity on micro- and nanoplastic particle (MNP) atmospheric half-lives. Half-lives of MNPs of different diameters (0.1 μm, 1.0 μm, 2.5 μm, 10 μm) in a 1 km atmosphere for **a** low-density polyethylene (LDPE) and **b** polyvinyl chloride (PVC) under different rain intensities (RI), where the uniform raindrop diameter D_p for each rain intensity is calculated as follows[83]: $D_p = 0.97e^{-3}$ x (RI x 0.158). Drizzle with RI < 0.5 mm h^{-1} (D_p = 0.87 mm), moderate rain with 0.5 mm h^{-1} < RI < 4 mm h^{-1} (D_p = 1.10 mm), heavy rain with 4 mm h^{-1} < RI < 8 mm h^{-1} (D_p = 1.35 mm), very heavy rain with RI > 8 mm h^{-1} (D_p = 1.40 mm).

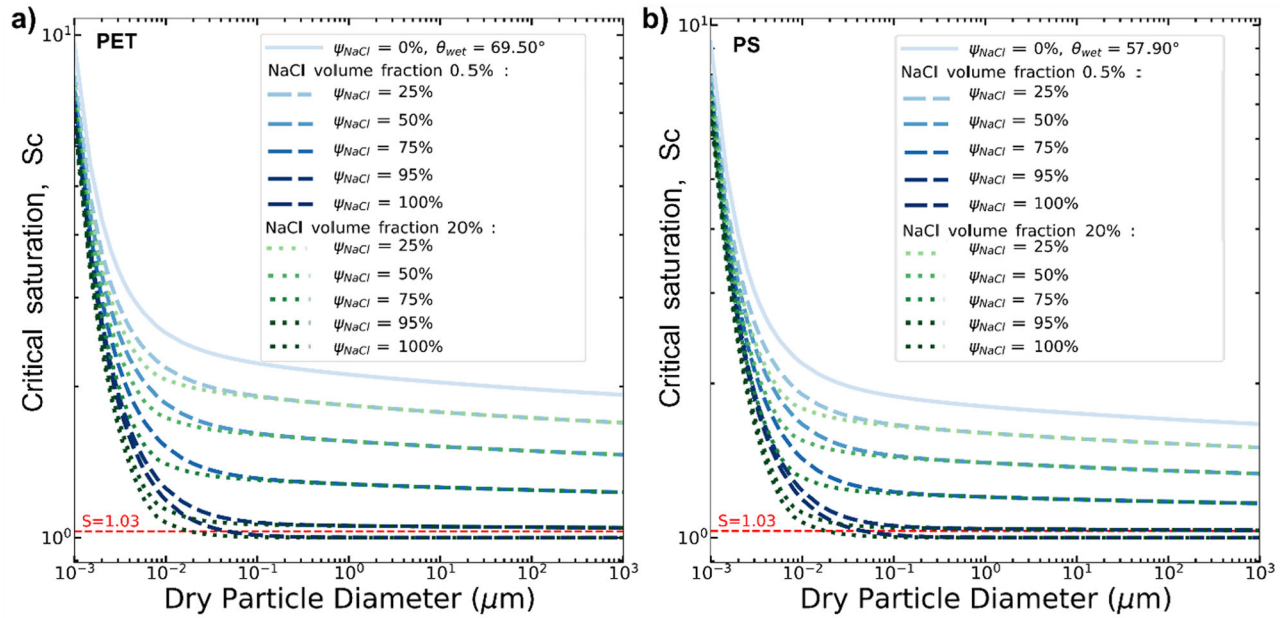

Fig. 8 | Impact of surface coverage ψ and volume fraction on the critical supersaturation (S_c) of weathered micro- and nanoplastic particles (MNPs). The coating's volume fraction is defined as the volume fraction of coating relative to the total volume of the particle and is proportional to the coating thickness. Here, calculated for sodium chloride (NaCl)-coated **a** polyethylene terephthalate (PET) and **b** polystyrene (PS) particles. Particles become capable of acting as cloud condensation nuclei (CCN) when the surface coverage exceeds 95%. Higher volume fractions reduce the dry particle diameter required to act as CCN, when the surface covering exceeds 95%.

Supplementary Table 8 and Supplementary Fig. 13). However, the lowest contact angles for photoaged plastics typically remain in the range of 60° to 80°, which is insufficient to make CNN. This applies to different types of plastic materials, regardless of (minor) differences in wettability. For example, while the S_c is generally higher for polyethylene terephthalate (PET) compared to polystyrene (PS) MNPs of the same size, for both MNPs the only realistic scenario in which the particle surfaces could gain sufficient wettability to act as CCN, is the adsorption of a substantial amount (>95 % surface covering) of hydrophilic ligands, such as salt (Fig. 8). Sorption of biofilm or humic acids may also perform the same function. This is possible after substantial environmental weathering.

Recent research indicates that MNPs can be more effective INPs than CCN[62,77]. Girlanda et al.[77] found that polyacrylonitrile (PAN) nanoplastics, as well as aged PS nanoplastics can be effective INPs. Ice nucleation may therefore represent a relevant in-cloud scavenging processes, under conditions in which MNPs are able to reach higher altitudes in the troposphere (where mixed-phase and ice clouds dominate) and after considerable atmospheric ageing. More

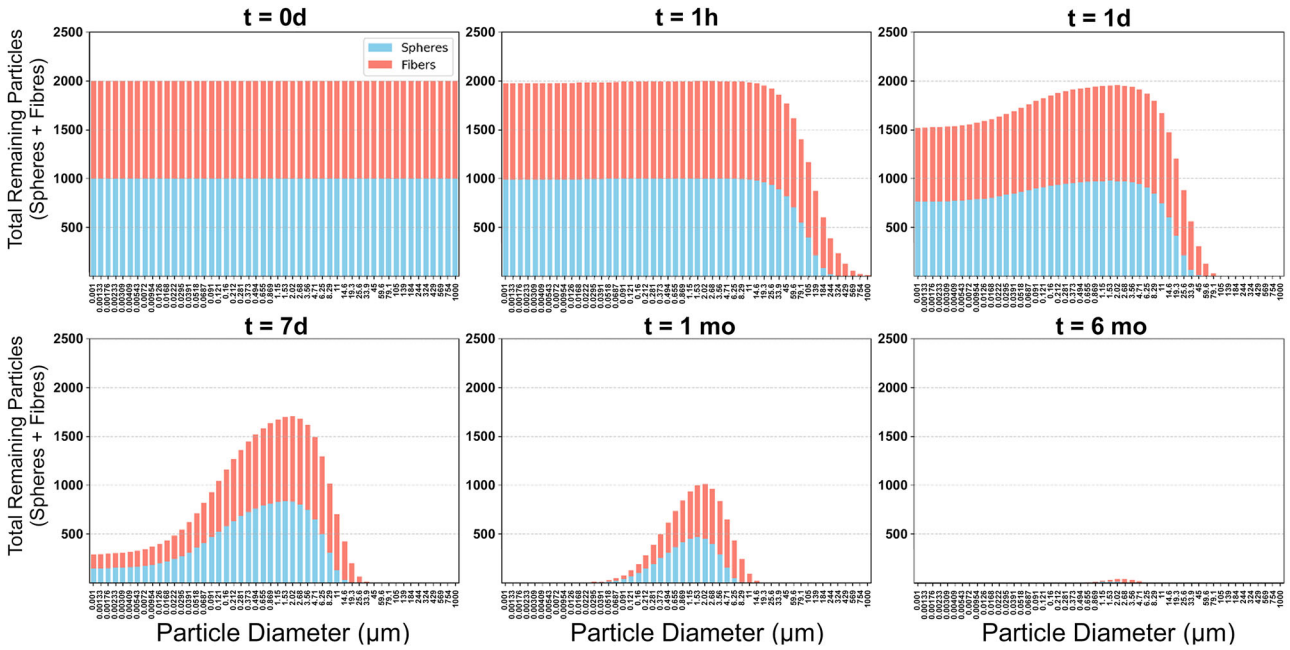

Fig. 9 | Evolution of a hypothetical heterogeneous micro- and nanoplastic particle (MNP) population over time. Initial particle population of low-density polyethylene (LDPE) MNPs is assumed to be composed of 50% spheres and 50% fibres at time $t = 0$, equally distributed over 50 size bins ranging from 0.001 μm to 1000 μm, evenly spaced on a logarithmic scale. For fibres, an aspect ratio L/S (longest [L] over shortest [S] axis) of 100 is assumed, and the size bins correspond to the equivalent sphere radius for LDPE. Changes in particle number over time (1 h, 1 day, 1 week, 1 month, 6 months) are displayed assuming dry deposition conditions (no precipitation) on a desert surface with surface winds $u_s = 2$ m s^{-1}.

empirical data for more MNP types and sizes are needed to include this process more explicitly in our model framework.

In conclusion, the removal of non-covered pristine MNPs from the atmosphere via wet deposition is primarily driven by below-cloud scavenging. This process scales with the intensity of the precipitation event and is most efficient for very small and very large MNPs. As for dry deposition, a clear minimum in the wet removal rate is expected for MNPs around 1 μm in size. Furthermore, weathered MNPs can act as CCN and INPs specifically if their surfaces are more than 95% covered by a hydrophilic material (e.g., salts from the ocean).

Overall atmospheric half-lives and implications for long-range transport of MNPs

Accounting for all the different deposition mechanisms, we observe that the estimated half-lives in air for MNPs can range from a few seconds to weeks (Figs. 2 and 6). The main drivers for these differences are particle size and shape, precipitation characteristics, atmospheric stratification, land surface features, and surface wind velocities. Similar to what is known for other atmospheric particles[43], the atmospheric residence time of MNPs at the global scale is expected to be strongly influenced by intermittent wet deposition events. In the absence of precipitation, the atmospheric fate of MNPs will be influenced entirely by dry deposition. Consequently, the interplay between the timing of atmospheric emissions and intermittent wet deposition is likely to play an important role in controlling LRAT potential for MNPs at a global level.

MNPs with a diameter of around 1 μm are expected to have the longest atmospheric residence times, as they are less efficiently removed by both dry and wet deposition compared to smaller and larger particles. These MNPs can exhibit half-lives of up to two weeks under dry conditions, which is sufficient for LRAT to occur from, for example, Europe to the Arctic during the summer, when prevailing air flow patterns favour transport to high latitudes[78]. This behaviour is in line with other atmospheric aerosols, which typically demonstrate peak residence times for diameters between 0.1 and 1 μm[79]. Smaller and larger MNPs are, however, less likely to be transported over such long distances, unless they undergo several cycles of deposition and re-entrainment (equivalent to the grasshopper effect described for persistent organic pollutants[48,80]).

Fibres are most likely to reach remote environments; because of their higher aspect ratios (i.e. longer fibres), they are predicted to remain aloft in the atmosphere for longer durations than spherical particles of similar mass (Fig. 9)[13]. The heterogeneity of MNP distributions in the atmosphere, in terms of size, density, shape, and ageing state, needs to be accounted for when predicting overall LRAT behaviour. Fractionation is expected for a heterogeneous MNP population over time, illustrated for a hypothetical uniform distribution of LDPE fibres and spheres in Fig. 9. An immediate drop out of larger particles is expected, followed by the gradual development of an approximately log-normal distribution with mode between 1 and 2 μm for both spheres and fibres after about 7 days.

We should further stress that the transport of particulates in the atmosphere is stochastic with strong dependence on spatial and temporal variations in meteorological conditions. Hence, even for the same type of particle, a high variability in transport distances is expected, influenced by the location and timing of emissions. In addition, more extreme high-intensity weather patterns occurring at low frequency, such as major storms (or longer drought periods), could play a disproportionate role in facilitating the LRAT of MNPs, although these are more difficult to predict. The LRAT of MNPs is controlled by a complex interplay between particle- and system-specific factors, and this complexity is exacerbated by the stochastic nature of atmospheric transport, making specific predictions challenging. However, it is possible to make broad generalisations about atmospheric residence times based on MNP size, shape, polymer type and particle surface modification for a set of prevailing atmospheric conditions. The theoretical framework presented here allows these factors to be integrated to predict net behaviours and to reveal the sensitivity of these net behaviours to specific factors. In order to predict LRAT potential, this model can be combined with information on spatial and temporal patterns of MNP emissions and vectors for atmospheric transport to understand source-to-receptor relationships. It should include a description of variability in local weather

patterns (surface winds, stratification, precipitation events), which will influence the ratio of atmospheric dispersal *versus* removal via deposition. Environmental fate and transport models at high spatial and temporal resolution are, thus, needed to disentangle the complex interplay between MNP and environmental drivers for LRAT. Such models should incorporate mechanistic descriptions of dry and wet deposition processes and differentiate between MNPs of different sizes and shapes, along the lines described here. Under certain conditions, polymer type may also be important, e.g. for the dry deposition of MNPs >10 μm and for wet deposition, where thermal conductivity of different materials can affect thermophoresis. Finally, MNP ageing behaviour can also be important. This might make some polymer types more likely to act as CCN and be prone to in-cloud scavenging.

Conclusions

Environmental fate and transport models with high spatial and temporal resolution are needed to disentangle the complex interplay between the specific properties of MNPs and the various environmental factors that influence their potential for LRAT. The mechanistic descriptions of dry and wet deposition processes presented here should be incorporated into such models, and resulting spatially-resolved exposure patterns could be confronted with measured environmental data once global monitoring networks based on harmonised sampling, measurement, and reporting protocols are more established[16].

We show how existing theories of atmospheric particle transport can be combined with empirical data on MNP properties and atmospheric processes to estimate atmospheric residence times for MNPs. This work demonstrates that considerable differences in atmospheric residence times can occur for different MNPs, depending on size, shape, and polymer composition. We estimate that MNPs between 0.1 and 2 μm (with densities of 900–1600 kg m^{-3}) will have relatively long residence times in air during dry periods, but that these can be efficiently scavenged (in the order of hours) during intermittent precipitation events. The theoretical framework introduced here, thus, enables a more robust and mechanistic approach that can account for the entire range of physicochemical properties of MNPs, including differences in particle size, shape, polymer type, as well as the influence of environmental ageing and transformation processes on the properties of the particle. In addition, the influence of land surface properties, atmospheric stratification, surface wind speed, and precipitation characteristics is accounted for explicitly. This makes it possible to estimate atmospheric half-lives of MNPs under seasonally- and spatially-varying atmospheric conditions. Whilst we have not explicitly evaluated the effects of parameter uncertainties on the predicted atmospheric residence times of MNPs, the sensitivity of predicted MNP behaviours is clearly illustrated, allowing the effects of parameter uncertainties to be evaluated when these are known.

Overall, we show that atmospheric half-lives can vary by several orders of magnitude, ranging from seconds to weeks, influenced by a combination of particle properties and system-dependent environmental factors. These insights need to be accounted for when evaluating LRAT for MNPs. In general, the atmospheric fate and transport of most MNPs is consistent with that of other atmospheric particles, including mineral dust and pollen. As with other particles, however, the complex mixture of properties associated with environmentally relevant MNPs, such as differences in density, surface properties (thermal conductivity and wettability) and shape, need to be explicitly included to improve the accuracy of mechanistic fate and transport descriptions. This is particularly important for fibres or MNPs that have been subjected to considerable environmental weathering. Longest atmospheric half-lives (and highest potential for LRAT) are estimated for spherical MNPs with diameters around 1 μm. Longer atmospheric residence times are expected for fibres than for spherical particles of equivalent mass. This is consistent with recent theoretical developments, experiments and monitoring[13,15].

The equations employed in this paper are fully accessible via a GitHub repository, where they are provided in Jupyter Notebook format. They enable the calculation of dry and wet deposition rates under specific conditions and can be incorporated directly into fate and transport models describing MNPs. This work, thus, represents an important point of reference for building and updating multimedia environmental transport models for both MNPs and other particles in the atmosphere more holistically.

Methods

Dry deposition velocity of smooth spherical MNPs

The dry deposition velocity (v_d) was estimated from the terminal dry settling (or gravitational settling) velocity (v_g), the aerodynamic resistance to deposition (R_a) and the surface resistance to deposition (R_s)[49–51]:

$$v_d = v_g + \frac{1}{(R_a + R_s)} \tag{3}$$

v_g was based on the dominant settling mode (Brownian, Stokes or Newtonian) for a given MNP size, as discussed in more detail in the Supplementary Information (see Supplementary Methods 1 and Supplementary Fig. 2 for how we determined the size threshold between different settling modes). For MNPs with a particle diameter d_p > 76 μm **Newtonian settling** dominates and v_g is estimated from[81]:

$$v_{g_{Newton}} = \sqrt{\frac{4 d_p g \left(\rho_p - \rho\right)}{3 C_D \rho}} \tag{4}$$

where ρ_p is the density of the MNP particle, ρ is the fluid density (here of air), C_D is the drag coefficient (unitless) and g is acceleration due to gravity. C_D depends on the Reynolds number Re (calculated for different flow regimes based on Kalman and Matana[82], see also Supplementary Table 2). For d_p between 76 and 17 μm we estimated v_g based on **Stokes Law**:

$$v_{g_{Stokes}} = \frac{g}{18\mu}\left(\rho_p - \rho\right) {d_p}^2 \tag{5}$$

where μ is the fluid viscosity. For d_p < 17 μm, v_g was calculated with Eq. 4 (with appropriate Re and C_D), but corrected using the Cunningham factor C_C[53] to account for the impact of **Brownian motion**:

$$v_{g_{Brownian}} = v_{g_{Newton}} C_C \tag{6}$$

with:

$$C_C = 1 + \frac{2\lambda}{d_p}\left(A_1 + A_2 \exp\left(\frac{-A_3 d_p}{2\lambda}\right)\right) \tag{7}$$

where λ is the mean free path of the fluid molecules and A_n are experimentally determined coefficients. Here, we used the coefficients proposed by Jennings[83] for air: $A_1 = 1.252$, $A_2 = 0.399$, $A_3 = 1.100$, $\lambda = 6.635 \times 10^{-8}$ m.

Dry deposition velocity of weathered MNPs

For weathered MNPs, or MNPs of different shapes, the difference between smooth and irregular surfaces can be introduced in Eqs. 4 and 5 via an empirical shape factor χ. For Newton's regime, the dry settling velocity becomes[81]:

$$v_{g_{Newton}} = \sqrt{\frac{4 d_p g \left(\rho_p - \rho\right)}{3 C_D \chi \rho}} \tag{8}$$

and for Stokes' regime (with $C_C = 1.0$) and the Brownian regime:

$$v_g = \frac{v_{g_{Newton}} C_C}{\chi} \tag{9}$$

For irregular rough surfaces (e.g. due to environmental weathering), we used χ=1.2 based on experimental measurements of spherical rough surfaces by Hassan and Lau[84]. Adjustments recommended for non-spheroidal shapes (e.g. cubes or plates) and MNP aggregates are described in Supplementary Methods 1.

Dry deposition velocity of MNP fibres

Fibres are flexible, with varying flatness and elongation[13,60]. During settling, they can adopt different orientations due to their flexibility (straight, semicircular, quarter circular, etc.). This flexibility leads to variations in Re and C_D, invalidating the approach, described above for weathered MNPs. Bagheri and Bonadonna[58] developed theoretical models for flexible fibres based on orientations (random, horizontal and average orientations), which are valid for a wide range of Reynolds numbers (up to $Re = 3 \times 10^5$). We adopt their average method, as it gives the best results compared to experimental measurements (as demonstrated by Tatsii et al.[60]). Details of the equations employed are provided in Supplementary Methods 1. As Re and C_D must be resolved in a self-consistent method, this increases computational time compared to other fixed shapes.

To compare spherical MNPs with MNP fibres, we used the equivalent volume (representing the same quantity of material, distributed in different shapes [Table 1]) and the aspect ratio *AR*, which is the longest axis *L* divided by shortest axis *S* (*AR* = *L*/*S*). Here, *L* is the length of a straight fibre and *S* is its diameter[60]. For a spherical MNP of diameter d_p, *S* and *L* of a fibre with the same equivalent volume is calculated based on its *AR* as follows:

$$S = \left(\frac{2.0 \times dp}{3.0 \times AR}\right)^{1/3} \tag{10}$$

$$L = AR \times S \tag{11}$$

Land surface and aerodynamic resistance to dry deposition

To account for the impact of land surface characteristics, atmospheric stratification and surface wind speed on dry deposition velocities we applied the resistance approach (Eq. 1), which is widely applied in physical and chemical transport models (see details in Supplementary Methods 2)[43,50,65]. We used the method and parameters introduced by Zhang et al[65]. for 15 land use categories (LUCs) (Supplementary Table 6) and two different surface wind velocities u_s (2 and 15 m s^{-1}). The impact of atmospheric stratification is accounted for by Zhang et al. [65] and detailed in Supplementary Methods 1.

Wet deposition velocity of MNPs

Removal of atmospheric MNPs by wet deposition occurs via below-cloud or in-cloud scavenging (Fig. 5).

Below-cloud scavenging of MNPs

Below-cloud scavenging is calculated using Eq. 2. The scavenging coefficient λ_p depends on raindrop diameter (D_p) and MNP diameter (d_p), their terminal velocities (*V* and *v*) and on the collision efficiency *E* between raindrop and MNP[51]:

$$\lambda_p = \int_0^\infty \frac{\pi}{4}\left(D_p + d_p\right)^2 \left(V\left(D_p\right) + v\left(d_p\right)\right) E\left(D_p, d_p\right) N(D_p) dD_p \tag{12}$$

where, $N(D_p)$ is the raindrop size distribution, which depends on rainfall intensity (RI) (Supplementary Methods 3, Eq. S31). In the present work we used four distinct uniform raindrop diameters D_p, corresponding to the median diameter of the raindrop size distribution expected for four different RI categories (Supplementary Methods 3, Eq. S32): (i) Drizzle with RI < 0.5 mm h^{-1} (D_p = 0.87 mm), (ii) moderate rain with 0.5 mm h^{-1} < RI < 4 mm h^{-1} (D_p = 1.1 mm), (iii) heavy rain with 4 mm h^{-1} < RI < 8 mm h^{-1} (D_p = 1.35 mm) and (iv) very heavy rain with RI > 8 mm h^{-1} (D_p = 1.4 mm).

The collision efficiency *E* is calculated from the contributions of Brownian diffusion (Eq. S33), interception (Eq. S38), impaction (Eq. S39), thermophoreris (Eq. S43), diffusophoresis (Eq. S46) and electrophoresis (Eq. S49)]. The relative contribution of these different processes to the overall *E* depends on MNP size (Supplementary Fig. 12), thermal conductivity, which is material- dependent (Supplementary Table 7) and on particle charge.

In-cloud scavenging of MNPs

In-cloud scavenging is governed by two mechanisms: collision scavenging of MNPs by waterdrops and nucleation scavenging, which involves MNPs acting as cloud condensation nuclei (CCN) or ice nuclei (IN) in a water-saturated atmosphere (Fig. 5). The likelihood of particle nucleation in a supersaturated environment, such as clouds depends on particle size, particle surface hydrophilicity and the relative humidity of the surrounding environment. The critical supersaturation S_c of a particle—i.e. the minimum level of supersaturation in a saturated medium required for a particle to grow or nucleate—can be derived with the Köhler equation[74,75].

For partially hydrophilic or mostly hydrophobic particles (as is the case for most pristine MNPs), the ability of the particle to act as a CCN depends on the contact angle for wettability (θ) between the MNP surface and water droplets[85,86]. S_c is expressed as a function of θ (for small θ)[87]:

$$S_c(d_p) = \left[\exp(A + W) - 1\right] \times 100\% \tag{13}$$

where *A*, is the S_c equilibrium water deposition term defined as:

$$A = \frac{4\sigma_w M_w}{RT\rho_w d_p} \tag{14}$$

in which *T* is the temperature, σ_w is the surface tension of the water film on the particle, M_w is the molecular weight of water, ρ_w is the density of water and *R* is the universal gas constant.

The S_c wettability term, *W* is defined as:

$$W = \frac{1 - \cos\theta}{\sqrt{0.662 + 0.022\ln(d_p/2)}} \tag{15}$$

Contact angles θ for pristine and photoaged MNPs adopted here can be found in Supplementary Table 8.

Impact of surface coverage

To calculate the effect of surface contamination of MNPs, e.g. with a hydrophilic coating such as NaCl (Fig. 8), we accounted for the volume of the coating, the hygroscopy of the coating material (including expansion due to water uptake) and the aqueous solubility of the coating. These factors can all affect nucleation scavenging. Thus, the definition of *A* in Eq. 14 was replaced by an extension of the Köhler theory[88], including terms to describe the wettability and the heterogeneity of the partially recovered MNP surface and incorporating Cassie's equation[89] for chemically heterogeneous surfaces (with possible different local contact angles). This leads to a revised definition of *A* as[88]:

$$A = \frac{d_T^3 - d_p^3}{d_T^3 - d_p^3(1-\kappa)} \exp\left(\frac{4\sigma_{(s,a)} M_w}{RT\rho_w d_T}\right) \tag{16}$$

where d_p is the volume equivalent diameter of the insoluble MNP, defined as $d_p = 6V_{MNP}/\pi$, in which V_{MNP} is the volume of the core MNP; d_T is the total volume equivalent diameter of the insoluble MNP and the core materials, defined as $d_T = 6V_T/\pi$ in which V_T is the total volume of the core MNP and the covering material, $\sigma_{(s,a)}$ is the surface tension of the solution/air interface and κ is a hygroscopicity parameter defined by the mixing rule:

$$\kappa = \sum_i \varepsilon_i \kappa_i H(x_i) \tag{17}$$

where i is the coating component considered, ε_i is its volume fraction, κ_i is the component hygroscopicity, and the dissolved volume fraction of the solute x_i and $H(x_i)$ defined as:

$$x_i = \left(g^3 - 1\right) C_i/\varepsilon_i, H(x_i) = \begin{cases} x_i \, x_i < 1 \\ 1 \, x_i \geq 1 \end{cases} \quad (18)$$

where g is a diameter growth factor defined as d_T/d_p, C_i is the solubility of the compound i in water (expressed as volume of compound per unit volume of water). The S_c wettability term, W, is then defined as:

$$W = \frac{1 - \cos(\theta_{\text{global}})}{\sqrt{0.662 + 0.022 \ln(d_T/2)}} \quad (19)$$

where the global contact angle θ_{global} is defined as:

$$\cos(\theta_{\text{global}}) = \sum_i f_i \cos\theta_i \quad (20)$$

in which f_i is the fractional area of the surface with a contact angle of θ_i

We assumed the following parameters in the illustrations presented here:

$\kappa_{PET} = 0.0$, $C_{PET} = 0.0$ m^3m^{-3}; $\theta_{PET} = 69.5°$ (from[76])

$\kappa_{NaCl} = 1.28$ (from[90]); $C_{NaCl} = 1.6 \times 10^{-1}$ m^3m^{-3} (from[91]), $\theta_{NaCl} = 0.0°$, where C_{PET} is the PET solubility and C_{NaCl} is the NaCl solubility.

Atmospheric half-lives: with first-order processes, with rate constant k, the half-life $t_{1/2}$ of a process is the time required for the concentration of particles to decrease to half of its initial value:

$$t_{1/2} = \frac{\ln(2)}{k} \quad (21)$$

Under dry conditions, dry deposition is a first-order process and the dry deposition rate constant for removal of MNPs (k_{dry}) can be calculated from the settling velocity v_d and the height of the atmospheric compartment z:

$$t_{1/2(dry)} = \frac{\ln(2)}{k_{dry}} = \frac{\ln(2)}{v_d/z} \quad (22)$$

Here, we assumed a value of 1 km for z in all calculations.

Under wet conditions, particles are removed from the atmosphere by both dry and wet deposition. Assuming that both of these processes can be described as first-order reactions the half-life under wet conditions is:

$$t_{1/2(wet)} = \frac{\ln(2)}{k_{dry} + k_{wet}} \quad (23)$$

where

$$k_{wet} = \frac{3}{2} \times E_{eff} \times \frac{RI}{D_p} \quad (24)$$

where D_p is the rain drop diameter, RI is the rainfall intensity and E_{eff} is the total sum of the collision efficiencies of a particle by a droplet (Brownian + Interception + Impaction + thermophoresis + Diffusiophoresis + electrophoresis collision efficiencies).

Reporting summary

Further information on research design is available in the Nature Portfolio Reporting Summary linked to this article.

Data availability

All model outputs used to generate the figures and derive the conclusions of this manuscript are available deposited on Zenodo (https://doi.org/10.5281/zenodo.17247014), together with input parameters and their sources.

Code availability

The information presented in this article has been compiled into an open-access framework available for the parameterisation of MNP transport models. The source code on GitHub (in Jupyter Notebook) is accessible via https://zenodo.org/records/17247014. The partial or complete extraction and use of the source code, is licensed under the Creative Commons 4.0 (CC BY) license.

Received: 23 December 2024; Accepted: 20 October 2025;
Published online: 27 November 2025

References

1. Thompson, R. C. et al. Twenty years of microplastic pollution research—what have we learned?. *Science* **386**, eadl2746 (2024).
2. Gouin, T. Addressing the importance of microplastic particles as vectors for long-range transport of chemical contaminants: perspective in relation to prioritizing research and regulatory actions. *Microplastics Nanoplastics* **1**, 14 (2021).
3. Rochman, C. M. et al. Rethinking microplastics as a diverse contaminant suite. *Environ. Toxicol. Chem.* **38**, 703–711 (2019).
4. Hartmann, N. B. et al. Are we speaking the same language? for a definition and categorization framework for plastic debris. *Environ. Sci. Technol.* **53**, 1039–1047 (2019).
5. Koelmans, A. A., Redondo-Hasselerharm, P. E., Mohamed Nor, N. H. & Kooi, M. Solving the nonalignment of methods and approaches used in microplastic research to consistently characterize risk. *Environ. Sci. Technol.* **54**, 12307–12315 (2020).
6. Sperling, L. H. *Introduction to Physical Polymer Science*. (John Wiley & Sons, 2015).
7. Allen, S. et al. Atmospheric transport and deposition of microplastics in a remote mountain catchment. *Nat. Geosci.* **12**, 339–344 (2019).
8. Evangeliou, N. et al. Atmospheric transport is a major pathway of microplastics to remote regions. *Nat. Commun.* **11**, 3381 (2020).
9. Allen, S. et al. Evidence of free tropospheric and long-range transport of microplastic at Pic du Midi Observatory. *Nat. Commun.* **12**, 7242 (2021).
10. Napper, I. E. et al. Reaching new heights in plastic pollution—preliminary findings of microplastics on Mount Everest. *One Earth* **3**, 621–630 (2020).
11. Brahney, J. et al. Constraining the atmospheric limb of the plastic cycle. *PNAS* **118**, e2020719118 (2021).
12. Evangeliou, N., Tichý, O., Eckhardt, S., Zwaaftink, C. G. & Brahney, J. Sources and fate of atmospheric microplastics revealed from inverse and dispersion modelling: From global emissions to deposition. *J. Hazard. Mater.* **432**, 128585 (2022).
13. Xiao, S., Cui, Y., Brahney, J., Mahowald, N. M. & Li, Q. Long-distance atmospheric transport of microplastic fibres influenced by their shapes. *Nat. Geosci.* **16**, 863–870 (2023).
14. O'Brien, S. et al. There's something in the air: a review of sources, prevalence and behaviour of microplastics in the atmosphere. *Sci. Total Environ.* **874**, 162193 (2023).
15. Chen, Q. et al. Long-range atmospheric transport of microplastics across the southern hemisphere. *Nat. Commun.* **14**, 7898 (2023).
16. Allen, D. et al. Microplastics and nanoplastics in the marine-atmosphere environment. *Nat. Rev. Earth Environ.* **3**, 393–405 (2022).
17. Dris, R. et al. Microplastic contamination in an urban area: a case study in Greater Paris. *Environ. Chem.* **12**, 592–599 (2015).
18. Wagner, S. et al. Tire wear particles in the aquatic environment - a review on generation, analysis, occurrence, fate and effects. *Water Res.* **139**, 83–100 (2018).

19. Yadav, V. et al. Framework for quantifying environmental losses of plastics from landfills. *Resour. Conserv. Recycling* **161**, 104914 (2020).
20. Serrano-Ruiz, H., Martin-Closas, L. & Pelacho, A. M. Biodegradable plastic mulches: impact on the agricultural biotic environment. *Sci. Total Environ.* **750**, 141228 (2021).
21. Vassilenko, E. et al. Domestic laundry and microfiber pollution: exploring fiber shedding from consumer apparel textiles. *PLoS ONE* **16**, e0250346 (2021).
22. O'Brien, S. et al. Airborne emissions of microplastic fibres from domestic laundry dryers. *Sci. Total Environ.* **747**, 141175 (2020).
23. Dris, R., Gasperi, J., Saad, M., Mirande, C. & Tassin, B. Synthetic fibers in atmospheric fallout: a source of microplastics in the environment?. *Mar. Pollut. Bull.* **104**, 290–293 (2016).
24. Allen, S. et al. Examination of the ocean as a source for atmospheric microplastics. *PLoS ONE* **15**, e0232746 (2020).
25. Harb, C., Pokhrel, N. & Foroutan, H. Quantification of the emission of atmospheric microplastics and nanoplastics via sea spray. *Environ. Sci. Technol. Lett.* **10**, 513–519 (2023).
26. Catarino, A. I. et al. Micro- and nanoplastics transfer from seawater to the atmosphere through aerosolization under controlled laboratory conditions. *Mar. Pollut. Bull.* **192**, 115015 (2023).
27. Wright, S. L., Gouin, T., Koelmans, A. A. & Scheuermann, L. Development of screening criteria for microplastic particles in air and atmospheric deposition: critical review and applicability towards assessing human exposure. *Microplastics Nanoplastics* **1**, 6 (2021).
28. Mountford, A. S. & Morales Maqueda, M. A. Modeling the accumulation and transport of microplastics by sea ice. *J. Geophys. Res. Oceans* **126**, e2020JC016826 (2021).
29. van der Does, M., Knippertz, P., Zschenderlein, P., Giles Harrison, R. & Stuut, J.-B. W. The mysterious long-range transport of giant mineral dust particles. *Sci. Adv.* **4**, eaau2768 (2018).
30. Kelly, J. T., Chuang, C. C. & Wexler, A. S. Influence of dust composition on cloud droplet formation. *Atmos. Environ.* **41**, 2904–2916 (2007).
31. Aylor, D. E. Settling speed of corn (Zea mays) pollen. *J. Aerosol Sci.* **33**, 1601–1607 (2002).
32. Zieger, P. et al. Black carbon scavenging by low-level Arctic clouds. *Nat. Commun.* **14**, 1–8 (2023).
33. Pisso, I. et al. The Lagrangian particle dispersion model FLEXPART version 10.4. *Geosci. Model Dev.* **12**, 4955–4997 (2019).
34. Liu, Y. et al. Influence of meteorological conditions on atmospheric microplastic transport and deposition. *Environ. Res.* **265**, 120460 (2025).
35. Fu, Y. et al. Modeling atmospheric microplastic cycle by GEOS-Chem: An optimized estimation by a global dataset suggests likely 50 times lower ocean emissions. *One Earth* **6**, 705–714 (2023).
36. Uzun, P., Farazande, S. & Guven, B. Mathematical modeling of microplastic abundance, distribution, and transport in water environments: a review. *Chemosphere* **288**, 132517 (2022).
37. Domercq, P., Praetorius, A. & MacLeod, M. The Full Multi: an open-source framework for modelling the transport and fate of nano- and microplastics in aquatic systems. *Environ. Model. Softw.* **148**, 105291 (2022).
38. MacLeod, M., Domercq, P., Harrison, S. & Praetorius, A. Computational models to confront the complex pollution footprint of plastic in the environment. *Nat. Comput Sci.* **3**, 486–494 (2023).
39. Kaandorp, M. L. A., Lobelle, D., Kehl, C., Dijkstra, H. A. & van Sebille, E. Global mass of buoyant marine plastics dominated by large long-lived debris. *Nat. Geosci.* **16**, 689–694 (2023).
40. Besseling, E., Quik, J. T. K., Sun, M. & Koelmans, A. A. Fate of nano- and microplastic in freshwater systems: a modeling study. *Environ. Pollut.* **220**, 540–548 (2017).
41. Quik, J. T. K., Meesters, J. A. J. & Koelmans, A. A. A multimedia model to estimate environmental fate of microplastic particles. *Sci. Total Environ.* **882**, 163437 (2023).
42. Mennekes, D. & Nowack, B. Predicting microplastic masses in river networks with high spatial resolution at country level. *Nat. Water* **1**, 523–533 (2023).
43. Farmer, D. K., Boedicker, E. K. & DeBolt, H. M. Dry deposition of atmospheric aerosols: approaches, observations, and mechanisms. *Annu. Rev. Phys. Chem.* **72**, 375–397 (2021).
44. Bennett, D. H., McKone, T. E., Matthies, M. & Kastenberg, W. E. General formulation of characteristic travel distance for semivolatile organic chemicals in a multimedia environment. *Environ. Sci. Technol.* **32**, 4023–4030 (1998).
45. Wegmann, F., Cavin, L., MacLeod, M., Scheringer, M. & Hungerbühler, K. The OECD software tool for screening chemicals for persistence and long-range transport potential. *Environ. Model. Softw.* **24**, 228–237 (2009).
46. Saxby, J., Beckett, F., Cashman, K., Rust, A. & Tennant, E. The impact of particle shape on fall velocity: implications for volcanic ash dispersion modelling. *J. Volcanol. Geotherm. Res.* **362**, 32–48 (2018).
47. Scheringer, M., Jones, K. C., Matthies, M., Simonich, S. & Meent, D. van de. Multimedia partitioning, overall persistence, and long-range transport potential in the context of POPs and PBT chemical assessments. *Integr. Environ. Assess. Manag.* **5**, 557–576 (2009).
48. Wania, F. & Mackay, D. Tracking the distribution of persistent organic pollutants. *Environ. Sci. Technol.* **30**, 390A–396A (1996).
49. Emerson, E. W. et al. Revisiting particle dry deposition and its role in radiative effect estimates. *Proc. Natl. Acad. Sci. USA* **117**, 26076–26082 (2020).
50. Slinn, W. G. N. Predictions for particle deposition to vegetative canopies. *Atmos. Environ.* **16**, 1785–1794 (1982).
51. Seinfeld, J. H. & Pandis, S. N. *Atmospheric Chemistry and Physics: From Air Pollution to Climate Change* (John Wiley & Sons, 2016).
52. Pruppacher, H. R., Klett, J. D. & Wang, P. K. Microphysics of clouds and precipitation. *Aerosol Sci. Technol.* **28**, 381–382 (1998).
53. Cunningham, E. On the velocity of steady fall of spherical particles through fluid medium. *Proc. R. Soc. Lond. Ser. A Containing Pap. A Math. Phys. Character* **83**, 357–365 (1910).
54. Dittmar, S., Ruhl, A. S., Altmann, K. & Jekel, M. Settling velocities of small microplastic fragments and fibers. *Environ. Sci. Technol.* **58**, 6359–6369 (2024).
55. Preston, C. A., McKenna Neuman, C. L. & Aherne, J. Effects of shape and size on microplastic atmospheric settling velocity. *Environ. Sci. Technol.* **57**, 11937–11947 (2023).
56. Kulkarni, P., Baron, P. A. & Willeke, K. *Aerosol Measurement: Principles, Techniques, and Applications* (John Wiley & Sons, 2011).
57. Lau, R. & Chuah, H. K. L. Dynamic shape factor for particles of various shapes in the intermediate settling regime. *Adv. Powder Technol.* **24**, 306–310 (2013).
58. Bagheri, G. & Bonadonna, C. On the drag of freely falling non-spherical particles. *Powder Technol.* **301**, 526–544 (2016).
59. Coyle, R., Service, M., Witte, U., Hardiman, G. & McKinley, J. Modeling microplastic transport in the marine environment: testing empirical models of particle terminal sinking velocity for irregularly shaped particles. *ACS EST Water* **3**, 984–995 (2023).
60. Tatsii, D. et al. Shape matters: long-range transport of microplastic fibers in the atmosphere. *Environ. Sci. Technol*. https://doi.org/10.1021/acs.est.3c08209 (2023).
61. Crowder, T. M., Rosati, J. A., Schroeter, J. D., Hickey, A. J. & Martonen, T. B. Fundamental effects of particle morphology on lung delivery: predictions of Stokes' law and the particular relevance to dry powder inhaler formulation and development. *Pharm. Res.* **19**, 239–245 (2002).
62. Aeschlimann, M., Li, G., Kanji, Z. A. & Mitrano, D. M. Potential impacts of atmospheric microplastics and nanoplastics on cloud formation processes. *Nat. Geosci.* **15**, 967–975 (2022).
63. Lin, M. Y. et al. Universality in colloid aggregation. *Nature* **339**, 360–362 (1989).

64. Senesi, N. & Wilkinson, K. J. *Biophysical Chemistry of Fractal Structures and Processes in Environmental Systems* (John Wiley & Sons, 2008).
65. Zhang, L., Gong, S., Padro, J. & Barrie, L. A size-segregated particle dry deposition scheme for an atmospheric aerosol module. *Atmos. Environ.* **35**, 549–560 (2001).
66. Andersson, C., Langner, J. & Bergstroumm, R. Interannual variation and trends in air pollution over Europe due to climate variability during 1958–2001 simulated with a regional CTM coupled to the ERA40 reanalysis. *Tellus B Chem. Phys. Meteorol.* **59**, 77–98 (2007).
67. Ghan, S. J. & Easter, R. C. Impact of cloud-borne aerosol representation on aerosol direct and indirect effects. *Atmos. Chem. Phys.* **6**, 4163–4174 (2006).
68. Gong, W. et al. Cloud processing of gases and aerosols in a regional air quality model (AURAMS). *Atmos. Res.* **82**, 248–275 (2006).
69. Zakey, A. S., Solmon, F. & Giorgi, F. Implementation and testing of a desert dust module in a regional climate model. *Atmos. Chem. Phys.* **6**, 4687–4704 (2006).
70. Wang, Y. Q., Zhang, X. Y. & Arimoto, R. The contribution from distant dust sources to the atmospheric particulate matter loadings at XiAn, China during spring. *Sci. Total Environ.* **368**, 875–883 (2006).
71. Heald, C. L. et al. Concentrations and sources of organic carbon aerosols in the free troposphere over North America. *J. Geophys. Res. Atmos.* **111**, (2006).
72. Duhanyan, N. & Roustan, Y. Below-cloud scavenging by rain of atmospheric gases and particulates. *Atmos. Environ.* **45**, 7201–7217 (2011).
73. Williams, A. L. Analysis of in-cloud scavenging efficiencies. in *Precipitation Scavenging ERDA Symp. Ser.., edited by RG Semonin, and RW Beadle* 258–275 (1977).
74. Köhler, H. *Zur Kondensation Des Wasserdampfes in Der Atmosphäre* (I kommission hos Cammermeyers boghandel Kristiania, 1921).
75. Köhler, H. *Zur Thermodynamik Der Kondensation an Hygroskopischen Kernen Und Bemerkungen Über Das Zusammenfliessen Der Tropfen* (Statens meteorologisk-hydrografiska anstalt, 1926).
76. Huang, Z. & Wang, H. Study on the impact of photoaging on the generation of very small microplastics (MPs) and nanoplastics (NPs) and the wettability of plastic surface. *Environ. Sci. Pollut. Res.* **30**, 92963–92982 (2023).
77. Girlanda, O., Li, G., Mitrano, D. M., Dreimol, C. H. & Kanji, Z. A. Ice nucleation onto model nanoplastics in the cirrus cloud regime. *Environ. Sci. Atmos.* **5**, 378–393 (2025).
78. Zheng, C. et al. Summertime transport pathways from different northern hemisphere regions into the Arctic. *J. Geophys. Res. Atmos.* **126**, e2020JD033811 (2021).
79. Pruppacher, H. R. & Klett, J. D. The atmospheric aerosol and trace gases. in *Microphysics of Clouds and Precipitation* (eds Pruppacher, H. R. & Klett, J. D.) 216–286 https://doi.org/10.1007/978-0-306-48100-0_8 (Springer Netherlands, Dordrecht, 2010).
80. Gouin, T., Mackay, D., Jones, K. C., Harner, T. & Meijer, S. N. Evidence for the "grasshopper" effect and fractionation during long-range atmospheric transport of organic contaminants. *Environ. Pollut.* **128**, 139–148 (2004).
81. Ghanem, A., Young, J. & Edwards, F. Settling velocity models applied to ballasted flocs - a review. *Saber* **25**, 247–253 (2013).
82. Kalman, H. & Matana, E. Terminal velocity and drag coefficient for spherical particles. *Powder Technol.* **396**, 181–190 (2022).
83. Jennings, S. G. The mean free path in air. *J. Aerosol. Sci.* **19**, 159–166 (1988).
84. Hassan, M. S. & Lau, R. W. M. Effect of particle shape on dry particle inhalation: study of flowability, aerosolization, and deposition properties. *AAPS PharmSciTech* **10**, 1252–1262 (2009).
85. Dusek, U., Reischl, G. P. & Hitzenberger, R. CCN activation of pure and coated carbon black particles. *Environ. Sci. Technol.* **40**, 1223–1230 (2006).
86. Ueda, S., Mori, T., Iwamoto, Y., Ushikubo, Y. & Miura, K. Wetting properties of fresh urban soot particles: evaluation based on critical supersaturation and observation of surface trace materials. *Sci. Total Environ.* **811**, 152274 (2022).
87. McDonald, J. E. Cloud nucleation on insoluble particles. *J. Atmos. Sci.* **21**, 109–116 (1964).
88. Petters, M. D. & Kreidenweis, S. M. A single parameter representation of hygroscopic growth and cloud condensation nucleus activity – Part 2: Including solubility. *Atmos. Chem. Phys.* **8**, 6273–6279 (2008).
89. Cassie, A. B. D. & Baxter, S. Wettability of porous surfaces. *Trans. Faraday Soc.* **40**, 546–551 (1944).
90. Petters, M. D. & Kreidenweis, S. M. A single parameter representation of hygroscopic growth and cloud condensation nucleus activity. *Atmos. Chem. Phys.* **7**, 1961–1971 (2007).
91. Sullivan, R. C. et al. Effect of chemical mixing state on the hygroscopicity and cloud nucleation properties of calcium mineral dust particles. *Atmos. Chem. Phys.* **9**, 3303–3316 (2009).
92. Ghan, S. J. & Schwartz, S. E. Aerosol properties and processes: a path from field and laboratory measurements to global climate models. *Bull. Am. Meteorol. Soc.* **88**, 1059–1084 (2007).
93. Hoose, C., Lohmann, U., Bennartz, R., Croft, B. & Lesins, G. Global simulations of aerosol processing in clouds. *Atmos. Chem. Phys.* **8**, 6939–6963 (2008).

Acknowledgements

Funding for this work was obtained from the European Chemical Industry Council (CEFIC) through the Long-Range Research Initiative (LRI) project ECO57 *μPLANET: microplastic long-range transport assessment and estimation tools*. We would like to extend our special gratitude to Prof. Judy Shamoun-Baranes and Prof. Markus D. Petters for stimulating discussions.

Author contributions

Marianne Seijo designed the study, collated the underpinning literature, established the model framework, wrote the code, generated all figures and co-wrote the first draft of the manuscript. Antonia Praetorius designed and supervised the study, provided feedback on the model framework and co-wrote the first draft of the manuscript. Micheal J. Whelan and Todd Gouin designed the study, provided feedback on the model framework and made several rounds of edits to the manuscript. All authors have edited and approved the final version of the manuscript.

Competing interests

The authors declare no competing interests.

Additional information

Supplementary information The online version contains supplementary material available at https://doi.org/10.1038/s43247-025-02930-w.

Correspondence and requests for materials should be addressed to Antonia Praetorius.

Peer review information *Communications Earth and Environment* thanks the anonymous reviewers for their contribution to the peer review of this work. Primary Handling Editors: Somaparna Ghosh.